Available online at www.sciencedirect.com

ScienceDirect

Ceramics International 39 (2013) 8833–8839

CERAMICS INTERNATIONAL

www.elsevier.com/locate/ceramint

Effect of starch addition on microstructure and properties of highly porous alumina ceramics

Sa Li, Chang-An Wang*, Jun Zhou

State Key Lab of New Ceramics and Fine Processing, School of Materials Science and Engineering, Tsinghua University, Beijing 100084, PR China

Received 11 April 2013; received in revised form 12 April 2013; accepted 22 April 2013
Available online 30 April 2013

Abstract

Porous alumina ceramics with ultra-high porosity were prepared through combining the gel-casting process with the pore-forming agent technique. Porosity and pore size distribution of the sintered bulks were evaluated with and without adding starch, respectively. In particular, the influences of starch addition on the properties, including thermal conductivity and compressive strength were studied. It was found that the incorporation of starch increased the nominal solid loading in the suspension and subsequently promoted the particle packing efficiency. The porosity is raised with increasing starch content from 0 to 30 vol%, which brings the decrease in thermal conductivity, whereas the compressive strength isn't seriously degraded. The further higher starch addition (40 vol%), however, would deteriorate the performance of the alumina porous ceramics. It is believed that the appropriate starch amount (lower than 30 vol%), working as a pore-forming agent, suppresses the driving force of densification without affecting the connections of neighboring grains while excessive starch amount would lead to the collapse of the porous structure.

Keywords: B. Porosity; C. Mechanical properties; C. Thermal conductivity; D. Al_2O_3; Gel casting

1. Introduction

Porous ceramics have attracted increasing interest due to their applications as separation media for molten metal, hot gases, a variety of liquid filtration processes and as catalyst supports, bone scaffolds, and electrodes in fuel cells [1–4]. A number of techniques have been developed to fabricate porous ceramics, including the direct foaming method, the sacrificial template method and the gel-casting method [5–10]. Each of these methods has its own merits and drawbacks. For example, reticulated porous ceramics produced by the polymer foam replication method can have ultra-high porosity with large interconnections; however, these materials often have poor mechanical properties because of the defects generated during the pyrolysis of the polymer foam. In addition, this method is only suitable for generating ceramics with relatively large pores with a size of several hundreds of microns, or even millimeter scale. Tape casting with pore-forming fugitive phases is also a commonly used method, owing to its simple processability, yet it is difficult to optimize the pore structure using this method. Since each technique has its own inherent advantages and disadvantages, many attempts have been made to combine those methods to fabricate samples with some mechanical and structural properties that cannot be attained by either method. Ramay et al. prepared porous hydroxyapatite scaffolds by combination of the gel-casting and polymer sponge methods, which provided a better control over the microstructure of scaffolds and enhanced their mechanical properties [11]. Mao and co-workers produced porous ceramics with tri-modal pores by foaming and starch consolidation [12]. The resulting materials consisted of a hierarchical structure with large-sized cells, moderate-sized pores in cell wall and small-sized voids among grains. However, the integration of gel-casting and pore former agents is rarely reported.

For more than decades, preparation of porous ceramics using starch as pore-forming agent is attracting more and more attention because of its chemical purity and easy burnout without any residue as well as good body-forming ability

*Corresponding author. Tel./fax: +86 10 62785488.
E-mail addresses: wangca@tsinghua.edu.cn, wangca@mail.tsinghua.edu.cn (C.-A. Wang).

0272-8842
http://dx.doi.org/10.1016/j.ceramint.2013.04.072

[13–15]. Lyckfeldt and Ferreirab reported starch consolidation casting as a new shaping technique that utilized the ability of starch to swell and gelatinize in water at high temperature [16]. Starch worked as pore-forming and body-forming agents simultaneously in the starch consolidation casting process. However, starch granules generally change their size as well as the shape due to its swelling in the aqueous suspension, and therefore it becomes difficult to determine the characteristics of the pores of the final porous ceramics. In this study, we report a novel technique that integrates gel-casting with pore-forming agents by adding starch into alumina/TBA slurries. Microstructure including pore morphology, and pore size distribution was characterized. Thermal and mechanical properties were also investigated. An explanation was given to clarify the mechanism of starch addition working in the processing as well.

2. Experimental procedure

As starting materials, Al_2O_3 powder (about 1 μm average diameter, Shanghai Chemical Regent Co., China) was used. Tert-butyl alcohol (TBA, Beijing Yili Chemical Co., Beijing, China) was used as shaping solvent and pore forming agent in the gel-casting process. Commercially available wheat starch was used as pore former agent and binder. Experiments were carried out using the as-received starch, without any subsequent processing. The average size of the spherical granule of starch was approximately 10 μm. A premix solution of monomers and cross linker was prepared in TBA with a concentration of 14.5 wt% of acrylamide (AM, $C_2H_3CONH_2$) and 0.5 wt% N,N′-methylenebisacrylamide (MBAM, $(C_2H_3CONH)_2CH_2$). Initiator and catalyst for gelation reaction were ammonium persulfate (APS) and N,N,N,N- tetramethylethylenediamine (TEMED), respectively. All chemicals used in this study are of analytical grade. The TBA-based gel-casting technique typically consists of preparing a liquid suspension (slurry), molding, drying, binder removal and sintering. Different amounts of starch added to the stabilized Al_2O_3 suspension were meseaured as a volume fraction of ceramic powders, ranging from 0% to 40%. Slurries with 15 vol% solid loading, including Al_2O_3 powders, starch, TBA, and acrylamide (AM) were prepared by ball milling for 5 h. To adjust the suspension to a proper flow ability during casting, selected citric acid solution was added into the slurries. After ball milling, initiator and catalyst were mixed into the slurry. The slurries were poured into molds and dried at 52 °C in nitrogen atmosphere. During the drying procedure, the polymerization of AM took place and the TBA gradually volatilized. Green bodies were then produced and finnally sintered at 1450 °C for 2 h.

Thermal gravimetric-differential scanning calorimetry (TG-DSC) analysis was performed using SDT Q600 (TA-Instruments) with air flow at a heating rate of 10 °C/min from room temperature to 1450 °C. Microstructure was observed using scanning electron microscope (SEM, JSM 6700 F, JEOL, Tokyo, Japan). Pore size distribution was analyzed by mercury intrusion porosimetry (AutoPore-IV9510, Micromeritics Instrument Corp., United States). Porosity was obtained from the ratio of the bulk density, measured from the samples' mass and dimensions, to the theoretical one of this Al_2O_3 material (3.98 g/cm^3). Three samples were examined to determine the average porosity. Linear shrinkage was obtained through recording the image changes on a sintering point testing device with screen display machine (SJY, Xiangtan Instrument and Meter Factory). A cubic sample with a dimension of $1 \times 1 \times 1$ mm^3 was heat treated from 50 to 1450 °C and the heating schedule was the same with the green body. Then we measured the size change and calculated the linear shrinkage based on a series of images got at a interval of 30 s during the sintering process. Thermal conductivity at room temperature was measured on $5 \times 5 \times 3$ mm^3 machined specimens, using Thermal Transport Option (TTO) of Physical Properties Measurement System (PPMS, Model 6000, Quantum Design, USA). For the compressive strength measurements, samples with 6 mm diameter and 12 mm height were loaded with a cross head speed of 0.05 mm/min (Instron 3369, Instron Corp.). Five specimens were used to obtain average values and standard deviations.

3. Results and discussion

In order to produce the desired porous ceramics without generating any defects, the organic phases (the starch and polymer) must be completely removed before sintering the alumina green bodies. To establish a heating schedule, TG/DSC analysis was carried out and the result is shown in Fig. 1(a). As revealed, the green body would go through weight reduction at two stages: a remarkable loss of about 30 vol% occurred at about 380 °C, and a following decrease continued at about 520 °C. The organic components were completely degraded at a temperature of < 600 °C. This result is confirmed by the DSC curve. A negligible amount of organic phases remained after the heat treatment. Based on this result, the optimized heating schedule for the sintering could be determined in Fig. 1(b). Samples were heated from 120 to 600 °C at a rate of 0.5 °C/min and maintained at this temperature for 2 h to remove the organic phases completely. Thereafter, the samples were sintered at 1450 °C for 2 h, followed by furnace cooling.

Fig. 2(a) and (b) respectively represents the SEM micrographs of the green bodies and the sintered compacts without adding any starch. Interconnected pores, which arise from the detachment of the solvent TBA during the drying process, are observed in the green body and amorphous materials exist between the spherical particles, which are polymer binders. Fig. S1(a, b and c) shows SEM micrographs of the original wheat starch granules, the wheat starch milled in TBA and water for 5 h, respectively. The mean granular size was approximately 10 μm before milling. When dissolved in water, starch would absorb water and generate fibrous structure (Fig. S1(c)). Such phenomenon has been applied in the starch consolidation, in which starch works as a body-forming agent to connect the ceramic powders together. However, after ball milling in TBA, the original large starch granules turn to regular small spherical particles with a diameter of about 2 μm. Fig. 1S(d) represents the micrograph of the mixture of alumina particles and starch granules after milled in the TBA for 5 h.

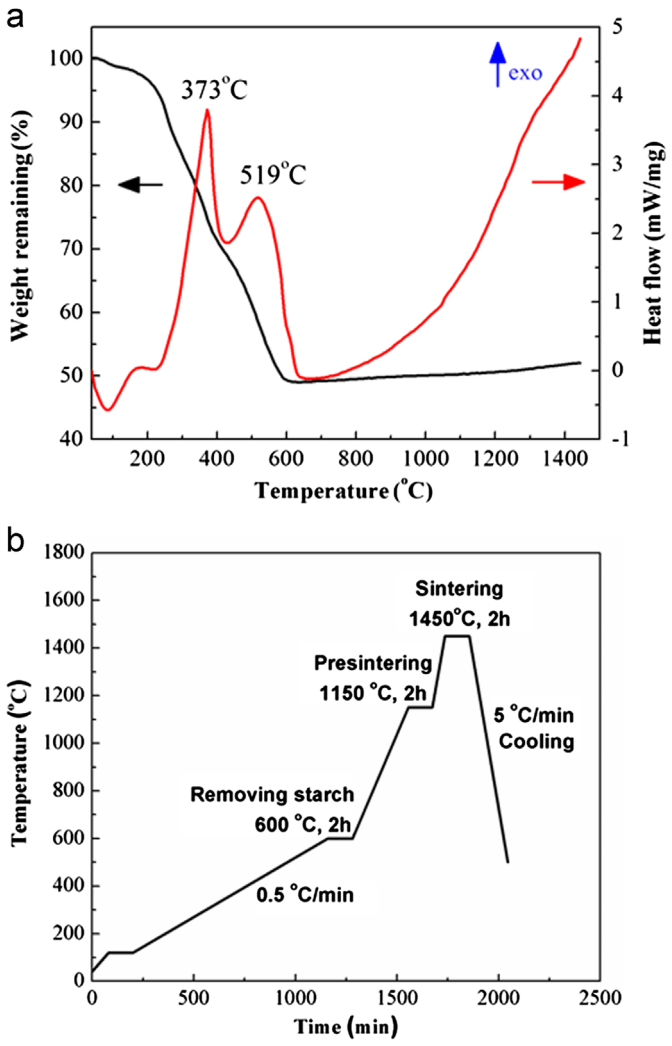

Fig. 1. (a) TG/DSC curves for thermal behavior of dried body in air and (b) the optimized thermal schedule.

As can be seen, these two kinds of solid particles are well mixed. After sintering at 1450 °C for 2 h, the amorphous materials disappear and the grains are connected to form a strong skeleton. When different amounts of starch were added into the slurry, although roughly identical grain connections also can be found in the sintered compacts, as revealed in Fig. 2(c)–(f), the pores dispersed in the alumina matrix are quite unlike in samples with various starch additions. Obviously, the most homogenous pore distribution is observed when the starch addition is 30 vol% while the pore size is not so uniform and larger pores as well as agglomerated particles occur in other cases. The mercury intrusion method was further used to verify the above observation of pore size distribution in the porous alumina ceramics with different starch additions. In Fig. 3, the curve of 30 vol% starch addition exhibits a sharpest increase from 0 to a stable value of cumulative volume, indicating monomodal and uniform pore size distribution. On the contrast, for the samples with higher or lower starch addition than 30 vol%, the upward trend seems to be sluggish and the total cumulative volume is lower, which indicates the broadening pore size distribution and the reduced pore volume. Despite the slight larger pores after adding starch, the total pore volume is significantly promoted and therefore higher porosity is expected in samples with adding starch.

Fig. 4a shows the relationship of the relative densities of both the green and the sintered compacts versus starch addition. A similar trend in relation to starch amount for both compacts is clearly illustrated. A linear decrease in density of green body with different starch contents was observed; however, for the sintered compacts, the density declined to a minimum value in the beginning, i.e. 0.75 g/cm^3, at 30 vol% starch addition, and rose to 0.89 g/cm^3 as the starch addition further increased to 40 vol%, which may result from pore collapse caused by starch removing. Furthermore, the variation of liner shrinkage of the porous alumina ceramics is investigated as a function of starch addition in Fig. 4b. As can be seen, the liner shrinkage of the samples firstly remained a similar level, about 19%, as the starch addition increased from 0 to 30 vol% and then went up rapidly to 26% at 40 vol% starch addition. It was believed that the sintering shrinkage is determined solely by the intergranular matrix porosity and the large pores resulting from starch burnout as well as the TBA eliminating process does not actively contribute to shrinkage [17]. From the porosity changes as a function of starch content in Fig. 4b, it can be seen that the porosity is raised with increasing starch content from 0 to 30 vol%. However, when the starch fraction exceeds 30 vol%, samples are incompletely sintered and therefore prone to crack, which means that there is an upper limit for starch content. Further adding of starch would lead to samples' cracking when the starch fraction exceeds the upper limit. As for samples without adding any starch, the porous structure is formed when TBA and polymer were eliminated at high temperature, approximately 600 °C, and then the two components traveled along numerous irregular channels from inside the ceramic to the surface. Once an appropriate amount of starch (lower than 30 vol%) was added into the suspension, it suppresses the driving force of densification without affecting the connections of neighboring grains. In this case, the porosity is increased with increasing starch addition while the linear shrinkage remains a similar level. On the contrary, excessive starch (i.e. 40 vol%) would lead to the collapse of the porous structure and therefore the opposite tendency of porosity and linear shrinkage is observed. In order to provide further evidence to support the above assumption, we investigate the relationship between linear shrinkage and the volume fraction at different heated stages before and after adding starch. As indicated in Fig. 5, the shrinkage rate starts later after adding starch, which is probably because of the larger average distance between alumina particles due to the interposition of starch granules in the green body

The above results demonstrate the microstructural development with adding starch and the subsequent changes in thermal and mechanical properties were investigated then. Fig. 6 shows the room-temperature thermal conductivity of porous alumina ceramics, together with the predicted values from the Maxwell–Eucken model and the EMT equation. On the basis of the

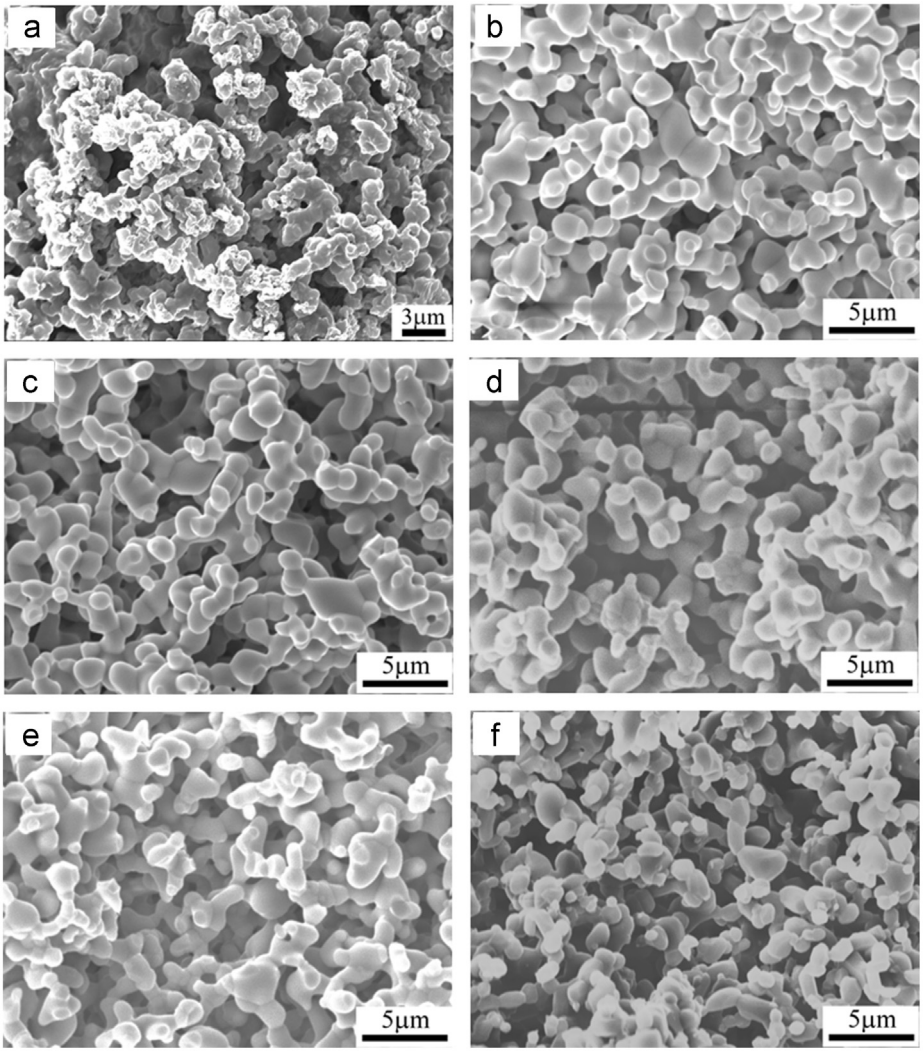

Fig. 2. SEM micrographs: (a) green body without starch and (b) sintered bulks with different starch additions (b) 0%, (c) 10%, (d) 20%, (e) 30%, and (f) 40%.

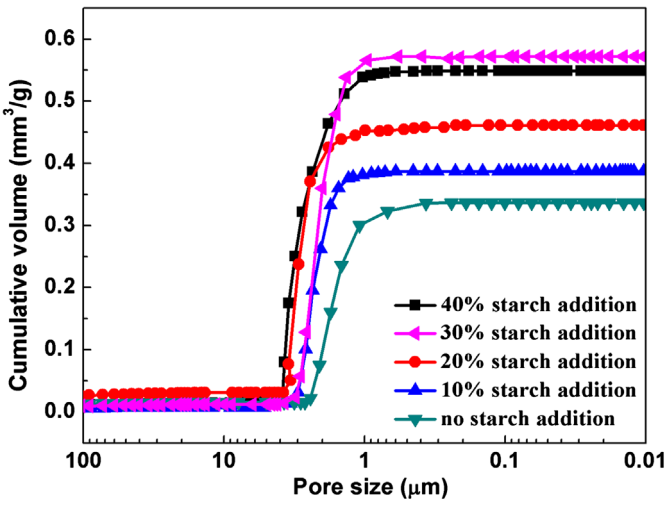

Fig. 3. Pore size distribution for porous alumina ceramics before and after adding starch.

component volume fractions and conductivities, Hashin and Shtrikman [18] derived effective conductivity bounds that were the best (i.e. narrowest) possible bounds for macroscopically homogeneous, isotropic, two-phase materials. Those bounds were mathematically equivalent to the two forms of the well-known Maxwell–Eucken model.

Maxwell–Eucken 1:

$$k_e = k_1 \frac{2k_1 + k_2 - 2(k_1 - k_2)v_2}{2k_1 + k_2 + (k_1 - k_2)v_2} \quad (1)$$

Maxwell–Eucken 2:

$$k_e = k_2 \frac{2k_2 + k_1 - 2(k_2 - k_1)(1 - v_2)}{2k_2 + k_1 + (k_2 - k_1)(1 - v_2)} \quad (2)$$

where k and v are thermal conductivity and volume fraction. Subscripts of e, 1 and 2 represent the two-component material, component 1 and component 2, respectively. The thermal conductivity of air and dense alumina ceramics were chosen to be 0.026 and 33 W/m K from literature values [19,20].

For a heterogeneous material structure in which the two components are distributed connectively, either component may form continuous heat conduction pathways, depending on the relative amounts of the components. James et al. [21] pointed out that the effective conductivity of this type of

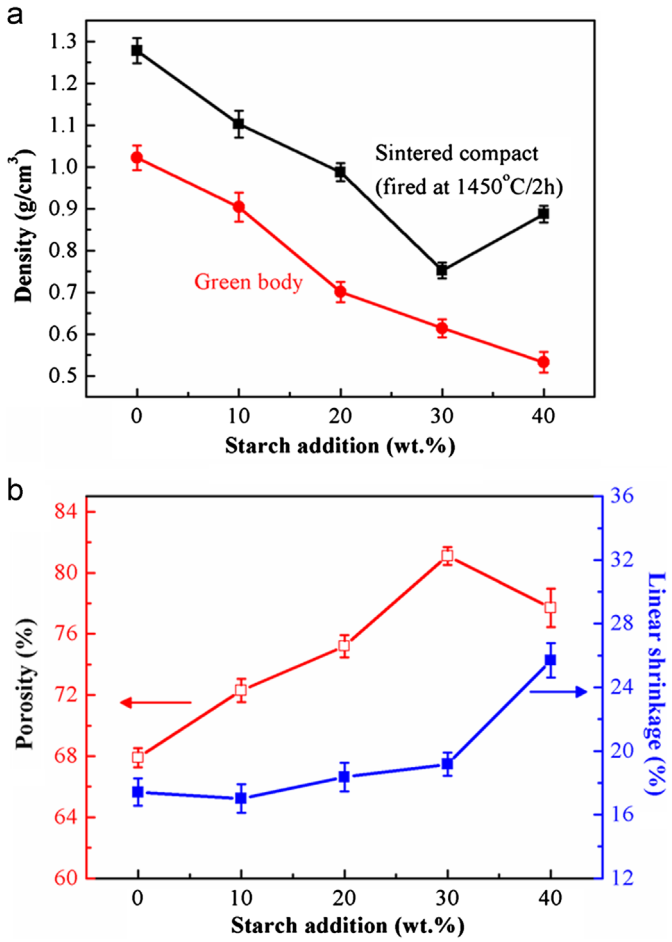

Fig. 4. (a) Relative density of the green body and sintered compacts vs. the starch addition and (b) porosity and linear shrinkage changes as a function of starch content.

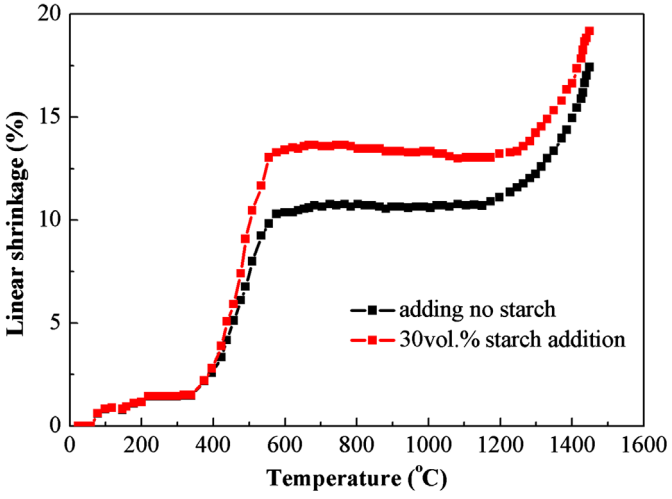

Fig. 5. The relationship between linear shrinkage for samples without adding starch and with 30 vol% starch addition.

structure could be modeled well by the EMT equation.

$$(1-v_2)\frac{k_1-k_e}{k_1+2k_e}+v_2\frac{k_2-k_e}{k_2+2k_e}=0 \quad (3)$$

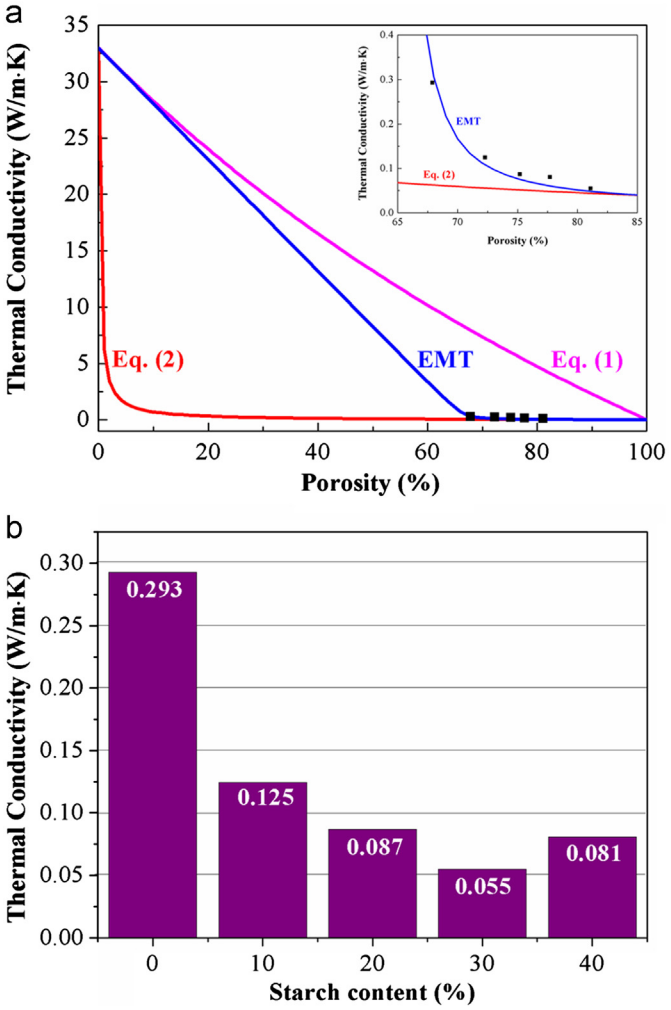

Fig. 6. (a) Comparison of experimental thermal conductivities and theoretical thermal conductivities based on the Maxwell–Eucken model and the EMT equation and (b) comparison of thermal conductivities of porous alumina ceramics with different starch contents.

The experimental thermal conductivities fit well with the values computed from the EMT equation, which gave values located between the bounds derived from the Maxwell–Eucken model. The initial thermal conductivity of fully dense alumina ceramics was about 33 W/m K [20]. In contrast, the thermal conductivity of porous alumina ceramic declined with increasing porosity, reaching a low value of 0.055 W/m K for the sample that had a porosity of 81.1%. The good agreement between the experiment data and EMT-calculated values may derive from the "interconnected" structure of porous alumina ceramics: pores and ceramic grains were distributed randomly, with neither component necessarily continuous or dispersed. Each component may form heat conduction pathways, depending on the volume fraction of the components. The effective conductivity of such an "interconnected" type of structure can be modeled well by the EMT equation, as established previously [22]. The observed decline in thermal conductivity with increasing starch addition could be explained by the microstructures developed within the porous alumina ceramics: the large number of pores trapped air, which is a better thermal

insulator (i.e., lower thermal conductivity) than alumina, and these air-filled pores constituted obstacles against the through-thickness heat transfer propagation; meanwhile, the large number of pores and micro-sized interfaces provided significant phonon and photon scatterings.

Fig. 7(a) shows the variation of compressive strength of porous Al_2O_3 ceramics with starch content. The increasing starch addition brought the higher porosity, but no apparent deterioration in compressive strength was found, indicating that no obvious change in the size of the effective or critical load-bearing area within the specimen. Generally, a number of expressions can be used to describe the compressive strength-porosity behavior of porous ceramics. One of the simplest methods was firstly proposed by Ryshkewitch [23] and Duckworth [24], and developed to be the *Rice* equation [25]:

$$\sigma = \sigma_0 \exp(-bP) \quad (4)$$

where σ_0 is the strength of a dense material, and σ is the strength of the porous material with a porosity of P, and b is a parameter depending on the structure and material composition.

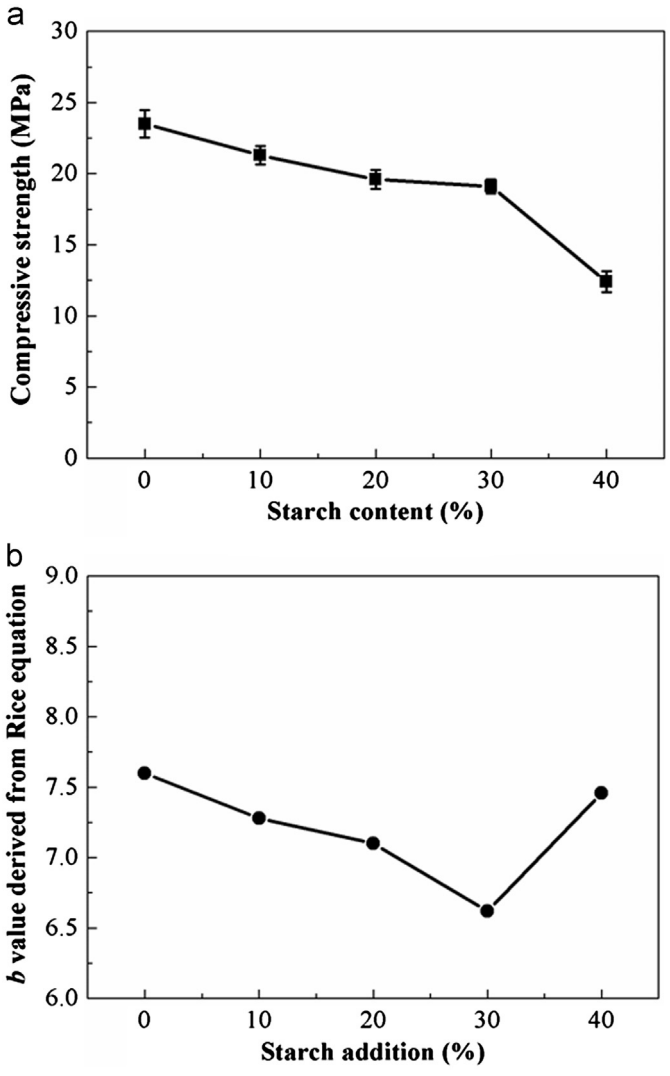

Fig. 7. Variation of compressive strength (a) and value of parameter b derived from the *Rice* equation (b) with different starch additions.

The value of the parameter b represents the susceptivity of strength on porosity, i.e. the larger b value, the more susceptivity of strength on porosity.

Attention has to be placed on the exponent parameter b because it indicates the susceptivity of strength on porosity. Fig. 7(b) shows the variation of the value of parameter b derived from the *Rice* equation (i.e. Eq. (4)). σ and P are the measured compressive strength and measured porosity of porous alumina ceramics. σ_0 is the compressive strength of dense alumina ceramics, which is taken as 4100 MPa for this Al_2O_3 material [26]. A slight decreasing trend of the value of parameter b with higher starch content was observed except for the sample added 40 vol% starch with an unexpected high value of parameter b, further verifying that similar grain interconnection is formed when the starch addition does not exceed 30 vol% while the skeleton becomes weak once the starch content reaches 40 vol%. The value of parameter b (6.6–7.6) calculated from Eq. (4) indicated a moderate porosity-dependent compressive strength of porous YSZ ceramics, by comparing to the corresponding values of some other porous ceramics (i.e. hydroxyapatite, $b=9.2$–10.8 [27]; YSZ, $b=7$ [24]; and mullite, $b=5.6$–6.2 [28]).

4. Conclusion

Porous alumina ceramics with ultra-high porosity were prepared through combining the gel-casting process with the pore-forming agent technique. It was found that the incorporation of starch increased the nominal solid loading in the suspension and subsequently promoted the particle packing efficiency. The porosity was raised with increasing starch content from 0 to 30 vol%, which caused the decrease in thermal conductivity, whereas the compressive strength was maintained at a relatively high value. The further higher starch addition (40 vol%), however, would deteriorate the performance of the alumina porous ceramics. It is believed that the appropriate starch (lower than 30 vol%), working as a pore-forming agent, suppresses the driving force of densification without affecting the connections of neighboring grains while excessive starch would lead to the collapse of the porous structure. This porous structure with ultra-high porosity is considered potentially useful in many applications such as heat-insulating structure, electrode in fuel cells and catalyst support.

Acknowledgments

The authors would like to thank the financial support from the National Natural Science Foundation of China (NSFC-Nos. 51172119 and 51102140).

Appendix A. Supporting information

Supplementary data associated with this article can be found in the online version at http://dx.doi.org/10.1016/j.ceramint.2013.04.072.

References

[1] L.J. Gauckler, M.M. Waeber, C. Conti, M. Jacobduliere, Ceramic foam for molten-metal filtration, Journal of Metals 37 (1985) 47–50.

[2] J. Coronas, J. Santamaría, Catalytic reactors based on porous ceramic membranes, Catalysis Today 51 (1999) 377–389.

[3] R. Faure, F. Rossignol, T. Chartier, C. Bonhomme, A. Maître, G. Etchegoyen, P.D. Gallo, D. Gary, Alumina foam catalyst supports for industrial steam reforming processes, Journal of the European Ceramic Society 31 (2011) 303–312.

[4] N.Q. Minh, Ceramic fuel cells, Journal of the American Ceramic Society 76 (1993) 563–588.

[5] A.R. Studart, U.T. Gonzenbach, E. Tervoort, L.J. Gauckler, Processing routes to macroporous ceramics: a review, Journal of the American Ceramic Society 89 (2006) 1771–1789.

[6] P. Sepulveda, Gelcasting foams for porous ceramics, American Ceramic Society Bulletin 76 (1997) 61–65.

[7] J. Saggio-Woyansky, C.E. Scott, W.P. Minnear, Processing of porous ceramics, American Ceramic Society Bulletin 71 (1992) 1674–1682.

[8] H.T. Wang, X.Q. Liu, G.Y. Meng, Porous α-Al_2O_3 Ceramics prepared by gelcasting, Material Research Bulletin 32 (1997) 1705–1712.

[9] J.L. Yang, J.L. Yu, Y. Huang, Recent developments in gelcasting of ceramics, Journal of the European Ceramic Society 31 (2011) 2569–2591.

[10] I.K. Jun, Y.H. Koh, J.H. Song, S.H. Lee, H.E. Kim, Improved compressive strength of reticulated porous zirconia using carbon coated polymeric sponge as novel template, Materials Letters 60 (2006) 2507–2510.

[11] H.R. Ramay, M.Q. Zhang, Preparation of porous hydroxyapatite scaffolds by combination of the gel-casting and polymer sponge methods, Biomaterials 24 (2003) 3293–3302.

[12] X.J. Mao, S.W. Wang, S.Z. Shimai, Porous ceramics with tri-modal pores prepared by foaming and starch consolidation, Ceramics International 34 (2008) 107–112.

[13] E. Gregorová, W. Pabst, I. Bohačenko, Characterization of different starch types for their application in ceramic processing, Journal of the European Ceramic Society 26 (2006) 1301–1309.

[14] E. Gregorová, W. Pabst, Porosity and pore size control in starch consolidation casting of oxide ceramics—achievements and problems, Journal of the European Ceramic Society 27 (2007) 669–672.

[15] E. Gregorová, W. Pabst, Z. Zivcová, I. Sedlárová, S. Holíková, Porous alumina ceramics prepared with wheat flour, Journal of the European Ceramic Society 30 (2010) 2871–2880.

[16] O. Lyckfeldt, J.M.F. Ferreirab, Processing of porous ceramics by starch consolidation, Journal of the European Ceramic Society 18 (1998) 131–140.

[17] E. Gregorová, W. Pabst, Process control and optimized preparation of porous alumina ceramics by starch consolidation casting, Journal of the European Ceramic Society 31 (2011) 2073–2081.

[18] Z. Hashin, S. Shtrikman, A variational approach to the theory of the effective magnetic permeability of multiphase materials, Journal of Applied Physics 33 (1962) 3125–3131.

[19] X.Q. Cao, R. Vasseh, D. Stoever, Ceramic materials for thermal barrier coatings, Journal of the European Ceramic Society 24 (2004) 1–10.

[20] W. Pabst, E. Gregorová, Effective thermal and thermoelastic properties of alumina, zirconia and alumina–zirconia composite ceramics, in: B.M. Caruta (Ed.), New Developments in Materials Science Research, Nova Science Publishers, New York, 2007, pp. 77–137.

[21] K.C. James, J.L. Simon, J.T. David, C.C. Andrew, Thermal conductivity bounds for isotropic, porous materials, International Journal of Heat and Mass Transfer 48 (2005) 2150–2158.

[22] B. Nait-Ali, K. Haberko, H. Vesteghem, J. Absi, D.S. Smith, Thermal conductivity of highly porous zirconia, Journal of the European Ceramic Society 26 (2006) 3567–3574.

[23] R. Ryshkewitch, Compression strength of porous sintered alumina and zirconia, Journal of the American Ceramic Society 36 (1953) 65–68.

[24] W. Duckworth, Discussion of Ryshkewitch paper by Winston Duckworth, Journal of the American Ceramic Society 36 (1953) 68.

[25] R.W. Rice, Comparison of stress concentration versus minimum solid area based mechanical property-porosity relations, Journal of Material Science 28 (1993) 2187–2190.

[26] C. Barleanu, Aspects concerning the ceramic surface accuracy in plane lapping, Mechanical Engineering 1 (1997) 433–438.

[27] D.M. Liu, Influence of porosity and pore size on the compressive strength of porous hydroxyapatite ceramics, Ceramics International 23 (1997) 135–139.

[28] A. Hattiangadi, A. Bandyopadhyay, Strength degradation of nonrandom porous ceramic structures under uniaxial compressive loading, Journal of the American Ceramic Society 83 (2000) 2730–2736.